Optical Engineering

SPIEDigitalLibrary.org/oe

Polarization signatures of airborne particulates

Prashant Raman
Kirk A. Fuller
Don A. Gregory

SPIE

Polarization signatures of airborne particulates

Prashant Raman
University of Alabama in Huntsville
Department of Physics
301 Sparkman Drive
Huntsville, Alabama 35899
E-mail: prashant.raman@gmail.com

Kirk A. Fuller
University of Alabama in Huntsville
Earth System Science Center
320 Sparkman Drive
Huntsville, Alabama 35805

Don A. Gregory
University of Alabama in Huntsville
Department of Physics
301 Sparkman Drive
Huntsville, Alabama 35899

Abstract. Exploratory research has been conducted with the aim of completely determining the polarization signatures of selected particulates as a function of wavelength. This may lead to a better understanding of the interaction between electromagnetic radiation and such materials, perhaps leading to the point detection of bio-aerosols present in the atmosphere. To this end, a polarimeter capable of measuring the complete Mueller matrix of highly scattering samples in transmission and reflection (with good spectral resolution from 300 to 1100 nm) has been developed. The polarization properties of *Bacillus subtilis* (surrogate for anthrax spore) are compared to ambient particulate matter species such as pollen, dust, and soot. Differentiating features in the polarization signatures of these samples have been identified, thus demonstrating the potential applicability of this technique for the detection of bio-aerosol in the ambient atmosphere. [DOI: 10.1117/1.OE.52.7.074106]

Subject terms: Mueller matrix; polarimetry; particulate matter; bio-aerosol; polarization; *B. subtilis*.

Paper 130011P received Jan. 3, 2013; revised manuscript received Jun. 18, 2013; accepted for publication Jun. 19, 2013; published online Jul. 17, 2013.

1 Introduction

Standoff detection of chemical or biological agents in the atmosphere is projected to be important in both rural and urban settings. This has focused research in the direction of early detection of airborne hazardous materials in particular. The importance of this endeavor, the many techniques employed, and the urgent need for improved technology are highlighted by Hurst and Wilkins.[1] Since no one technique is currently capable of completely differentiating between hazardous and nonhazardous materials, multiple techniques may have to be employed in tandem and active research is ongoing toward exploiting polarimetric techniques for particulate detection. A few experimental studies aimed at measuring the polarization state of scattered light from particulate matter (PM) species have been done but they are mostly limited to discrete wavelengths in the visible and infrared (IR) regions; emission lines between 9.1 and 12.1 μm from a CO_2 laser.[2] Spectral measurements of polarization properties of such samples over a broad wavelength region and at a high spectral resolution are scarce, primarily due to lack of available instrumentation.

A Mueller matrix spectropolarimeter (MMSP) that operates in transmission mode (MMSP-T) and reflection mode (MMSP-R) has been developed that is capable of determining all 16 elements of the Mueller matrix. The diattenuation (linear and circular), retardance (linear and circular), and depolarization properties of the sample are calculated from the Mueller matrix. This system seamlessly spans the 300- to 1100-nm spectral region and has been described, characterized, and reported earlier.[3] The earlier research has primarily focused on probing a plume of PM *in situ* with a specific state of polarized light and detecting the states of polarized light scattered from the plume akin to a polarization-based LIDAR system. The present research approaches the measurement in a different manner wherein the PM is deposited on glass substrates and measurements are performed in transmission and reflection. This approach could be useful in developing a dedicated polarimeter with an aerosol sampler. This research provides the complete spectral polarization signatures of various PM species and demonstrates the utility of the polarimeter for PM discrimination. Other point detection methods are discussed in the literature.[4]

Table 1 provides a list of several polarimeters developed in the recent past for characterizing aerosols in general, with some intended specifically for detecting bio-aerosols. The operating wavelengths and other design/operation characteristics are highlighted along with the references.

2 Definitions

The polarization state of the incident light invariably undergoes a change when it interacts with matter. There are essentially three different effects a polarizing element can have on incident light, namely, diattenuation, retardation, and depolarization. The optical elements that manipulate incident light in one of the above three ways are called diattenuators (or polarizers), retarders, and depolarizers, respectively. The samples considered here exhibit a combination of the above three polarization characteristics. A brief description of these polarization terms will be given and the details are given in the literature.[16,17]

Diattenuation refers to the different amounts of attenuation experienced by two orthogonal states of polarization. The attenuation is maximum for one state and minimum for its corresponding orthogonal state. Linear diattenuation and circular diattenuation refer to the diattenuation experienced by a pair of orthogonal linear and circular states, respectively. The diattenuation (D) is quantitatively defined as

$$D = \frac{I_{\max} - I_{\min}}{I_{\max} + I_{\min}}, \tag{1}$$

Table 1 Comparison of polarimeters developed for aerosol research.

Instrument	Wavelength	Descriptors	Parameters	References
Differential absorption Mueller matrix spectrometer (DIAMMS)	9.1 to 12 μm	Standoff, Active, Nonimaging, Backscattering	Sixteen elements of Mueller matrix	2 and 5
Standoff aerosol active signature testbed (SAAST)	1.35 to 5 μm	Standoff, Active, Nonimaging, Multiangle		6 and 7
Standoff polarimetric aerosol detection (SPADE)	1.5 μm, 2.12 μm	Standoff Active Nonimaging, Multiangle	Four elements of Stokes vector	8
Raman-shifted eye-safe aerosol LIDAR (REAL)	1.5 μm	Standoff, Active, Nonimaging	Linear polarization	9
Aerosol polarimeter sensor (APS)	412, 443, 555, 672, 865, 910, 1378, 1610, 2250 nm	Standoff, Passive, Nonimaging, Multiangle	Linear polarization	10
Airborne multiangle spectropolarimetric imager (AirMSPI)	470, 660, 865 nm	Standoff, Passive, Imaging, Multiangle	Linear polarization	11
Spectropolarimeter for planetary exploration (SPEX)	400 to 800 nm	Standoff, Passive, Imaging	Linear polarization	12
Polarimetric LIDAR	355, 532, 1064, 1570 nm	Standoff, Active, Nonimaging	Depolarization	13
Bio-aerosol ranging spectrometer (BARS)	1.06 μm (LIDAR)	Standoff, Active LIDAR/Passive Spectrometer, Nonimaging		14
Mueller matrix spectropolarimeter (MMSP)	300 to 1100 nm	Point detection, Active, Nonimaging	Sixteen elements of Mueller matrix	15

where $I_{\max}$ and $I_{\min}$ refer to the irradiances of the orthogonal polarization states. Diattenuators with $D = 1$ qualify to be called pure polarizers.

Orthogonal polarization states may experience a differential phase change, and the phase difference between the two orthogonal states (δ) is called retardance. Retardance can be induced through different mechanisms like birefringence and total internal reflection. For a retarder based on birefringence, retardance is given by

$$\delta = \frac{2\pi}{\lambda}\Delta n\, d, \tag{2}$$

where $\Delta n = |n_1 - n_2|$ is the birefringence or the difference in the refractive indices for a pair of orthogonal polarization states and d is the propagation length of the light within the birefringent material.

Depolarization refers to the process of turning polarized light into unpolarized light. An ideal depolarizer transforms any incident state of polarization into randomly polarized light. The degree of polarization of light exiting an ideal depolarizer equals zero. The depolarization index is quantified as[17]

$$\mathrm{Dep}(M) = 1 - \frac{\sqrt{\sum_{i,j} m_{ij}^2 - m_{00}^2}}{\sqrt{3}m_{00}}, \tag{3}$$

where M is the Mueller matrix and m_{ij} are the Mueller matrix elements. $\mathrm{Dep}(M) = 0$ corresponds to a nondepolarizing sample whereas $\mathrm{Dep}(M) = 1$ indicates an ideal depolarizing sample.

3 System Description

The MMSP developed in this research program is based on the dual rotating retarder architecture proposed by Azzam.[18] This robust architecture is capable of providing all 16 elements of the Mueller matrix. The calibration routines and data reduction schemes are well established.[19–22] The detailed description of the MMSP-T along with the calibration results and performance is detailed in the conference proceeding.[3] With respect to the design, the MMSP-R is identical to that of MMSP-T except that the light exiting the polarization state generator (PSG) is incident on the sample at an angle of 70 deg and the polarization state analyzer (PSA) is set up to receive the specular reflection from the sample. This corresponds to an effective scattering angle of 40 deg. In its current form, reconfiguring the MMSP from one mode of operation to another involves a significant amount of meticulous realignment and recalibration. Hence, a 70-deg incident angle was chosen allowing measurements on certain samples to be comparable to measurements using conventional ellipsometers. Measurements at other scattering angles are of interest chiefly in order to determine the optimum scattering angle leading to a better differentiation and enhanced sensitivity. Measurements using the current system are limited to a single scattering angle. An instrument incorporating in its design an easy way to change the scattering angle has been proposed for the next generation of MMSP along with the other improvements.[23] A system description

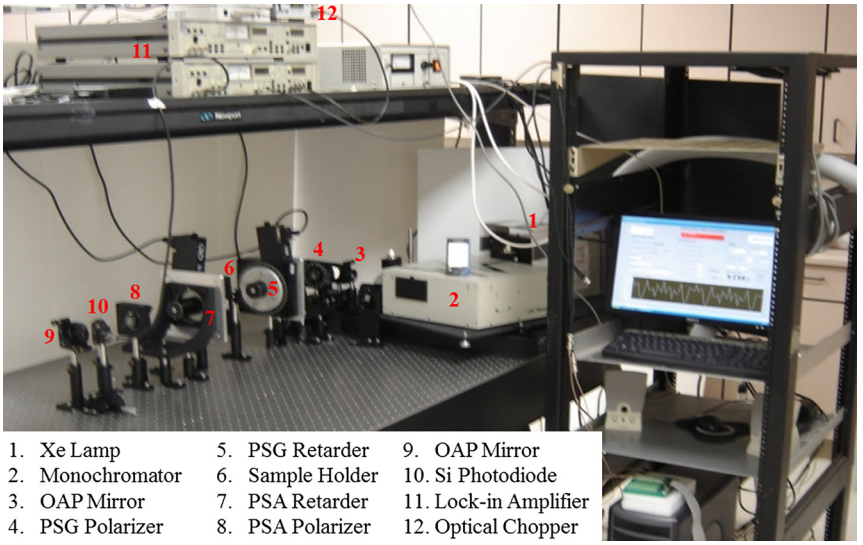

Fig. 1 Photograph of the Mueller matrix spectropolarimeter in transmission mode (MMSP-T).

of the MMSP-R and some experimental results are available in the literature.[15] Figure 1 is a photograph of the entire polarimeter configured in the MMSP-T. Figure 2 is a photograph highlighting the PSG and PSA subsystem of the polarimeter in MMSP-R. The MMSP is operated from 300 to 1100 nm at a 10-nm resolution.

4 System Validation

The MMSP-T was calibrated and validated against a retarder measured independently by two different research groups using different polarimeters. The magnitude of retardance measured by the current MMSP-T is within a degree of agreement with the other measurements.[3] In order to validate the performance of the MMSP-R, the reflection from a borosilicate microscope slide was measured. Reflection from a dielectric surface produces linear diattenuation. Utilizing the refractive index provided for borosilicate material in the Schott catalog[24] over the desired wavelength region and the Fresnel equations, the diattenuation between the s- and p-polarization states is calculated for a narrow range of incident angles (70 ± 1 deg) to take into consideration the influence due to possible misalignment of the slide in the sample space. Figure 3 is a plot of the theoretical and measured values of linear diattenuation of the microscope slide. The shaded area corresponds to the theoretically calculated diattenuation values over the range of incident angles. The solid black line corresponds to the measured values of diattenuation. Clearly, the measured values are mostly within the range of the theoretically calculated values. The width of this area corresponds to a possible ± 1 deg misalignment of the sample.

5 Measurements and Results

The range of PM samples on which measurements was performed include kerosene soot, two soil samples, three different species of pollen, and *Bacillus subtilis* (BG). BG is a well-known surrogate for anthrax spores and has been extensively used in the research.[25,26] The optical characteristics of bio-aerosols in general and *B. subtilis* in particular can be found in Refs. 27 and 28. The soot, soil, and pollen samples

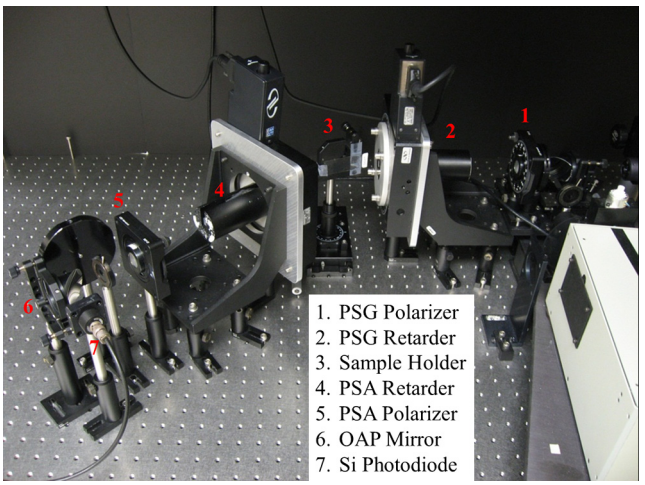

Fig. 2 Photograph of the polarization state generator (PSG) and polarization state analyzer (PSA) subsystem of MMSP in reflection mode (MMSP-R).

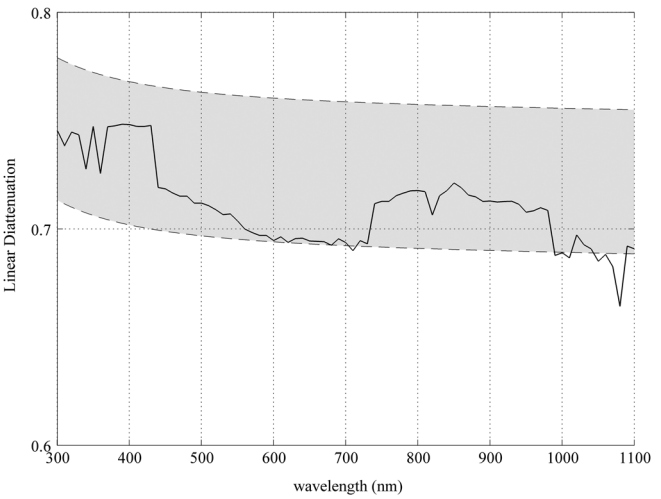

Fig. 3 Theoretically calculated diattenuation due to reflection from microscope slide.

represent major constituents of the ambient atmospheric aerosol, and can be considered interferants in the bio-aerosol (in this case BG) detection process. An example of the raw Mueller matrix data for the PM species is given in Fig. 4.

It was not possible to prepare samples consistently and uniformly; however, this inconsistency circumvents any measurement artifacts caused by an identical sample preparation. This inconsistency would appear in any real-world application of the technique. The different species of PM were measured in the transmission mode. Most of the polarization features of the aerosol species examined were found to be negligible (comparable to the measurement made on a blank slide) and hence, those results are not presented here. This is to be expected. Forward scattering from scattering particles provides significant throughput for measuring irradiance but no significant polarization content to measure. Hence, polarimetric measurements in the transmission mode cannot be expected to provide the required polarization features needed for differentiating the various aerosol species.

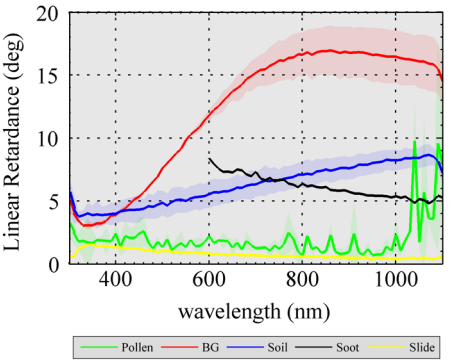

Fig. 5 Linear retardance of the PM species.

In reflection mode, the polarization signatures of the different PM species display significant differentiating features as can be seen in Figs. 5–8. The differentiating features seen in these measurements are a consequence of the differences in the size, shape, and optical constants of the scattering

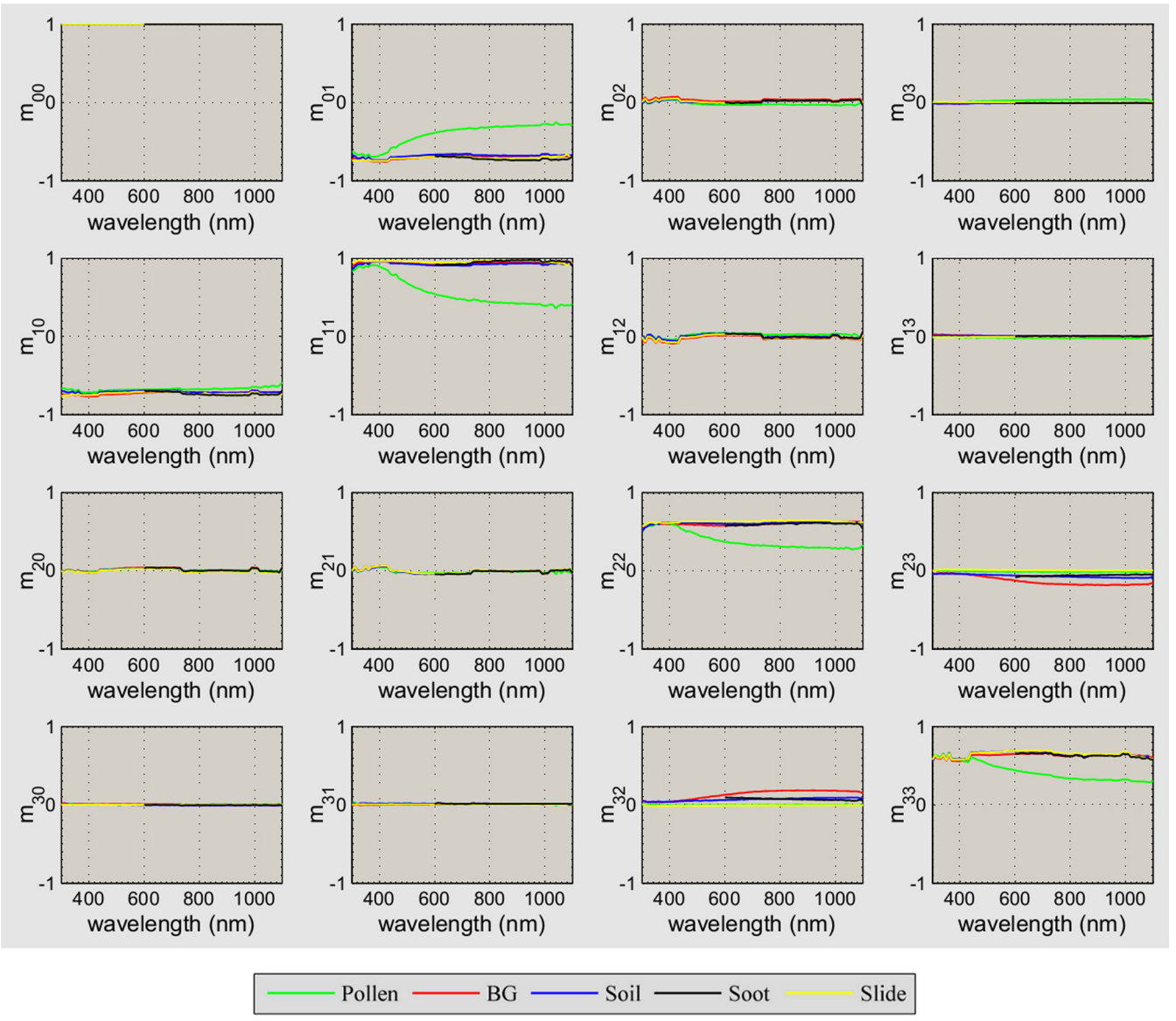

Fig. 4 Spectral Mueller matrix plot of the particulate matter (PM) species.

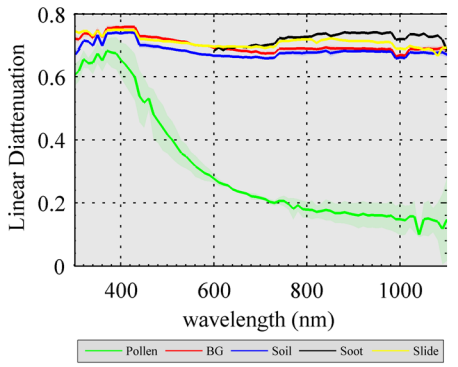

Fig. 6 Linear diattenuation of the PM species.

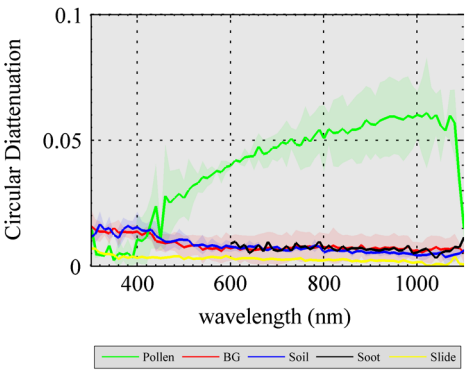

Fig. 7 Circular diattenuation of the PM species.

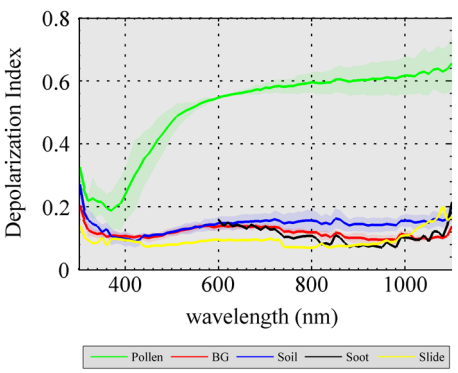

Fig. 8 Depolarization index of the PM species.

material. The exact correlation of the morphology and material properties with the measured polarization properties of the scattering particulates was unclear. However, Table 2 summarizes the morphology and material description[29–33] of the particulates which might contribute to such a correlation. The complex refractive index of particulates has been retrieved using an inversion algorithm[34,35] which may help validate the existing and future phenomenological studies.

The average polarization property (indicated in each figure) of the three types of pollen is plotted in green along with the standard deviation shown by the green shaded area. Similarly, the average of multiple measurements performed on BG and soil samples are plotted in red and blue, respectively, with the shaded areas corresponding to their standard deviations. The polarization property of kerosene soot is plotted in black and that of the blank microscope slide is plotted in yellow. In plots where the shaded area is not easily visible, the magnitude of standard deviation is comparable to the width of the corresponding line itself.

The polarization properties for the PM species are in stark contrast to each other. Although the linear retardance of pollen is comparable to the blank slide (in yellow), the linear diattenuation of pollen gradually decreases from ~0.7 at 400 nm to ~0.2 at 1100 nm. This is in contrast to the linear diattenuation of all the other PM species, as well as the blank slide. The decrease in linear diattenuation is accompanied by an increase in circular diattenuation, although of much smaller magnitude. Also, the depolarization due to pollen increases from ~0.2 at 400 nm to >0.5 at 1100 nm. The circular diattenuation of all other samples are negligibly small. Similarly, the depolarization indices of these samples are <0.2 over the entire spectral region and featureless. Differentiating polarization features in soil and soot samples can be seen in linear retardance. The soil sample displays an increase in the linear retardance from ~4 deg at 300 nm to ~9 deg at 1100 nm. The increase also appears to be quite linear in nature. Soot, on the other hand, has a decreasing linear retardance varying from ~8 deg at 600 nm to ~5 deg at 1100 nm. The narrower spectral range over which the polarization properties of soot is measured due to the fact that at the shorter wavelengths, the throughput was too low to be able to make reliable measurements or estimations of polarization properties. Nevertheless, the polarization

Table 2 Physical characteristics of particulates.

Particulate	Species/type	Size	Shape	Material description
Pollen	Nettle	~20 μm	Spheroidal	Cellulose (with protective wall)
	Ragweed	~20 μm	Spheroidal	Cellulose (with protective wall)
	Pine	~50 μm	Bisaccate	Cellulose (with protective wall)
Soil	Construction site	<50 μm	Irregular	Mainly crystalline mineral
	Baseball field	<50 μm	Irregular	Mainly crystalline mineral
Soot	Kerosene	~0.1 μm	Sphere cluster	Carbon (with traces of organics)
Bio-aerosol	*Bacillus subtilis*	5 μm rods	Clustered	Polymer of sugars and amino acids

signatures of PM species typically found in the ambient atmosphere have been completely determined.

Finally, *B. subtilis* or BG (surrogate for anthrax spore) is considered as representative of a serious airborne biohazard. It can be seen from Fig. 5 that BG has linear retardance that is nonlinear over the measured spectral region spanning 300 to 1100 nm in contrast to the other PM species. This trait may be useful in discrimination.

6 Conclusions

The complete Mueller matrix and polarization signatures of various PM species have been determined for the first time. The polarization properties of these samples have been determined over the wavelength range 300 to 1100 nm at a resolution of 10 nm. To take these measurements, a one-of-a-kind polarimeter (MMSP) was built which was proven versatile for performing measurements on a variety of samples for a wide range of applications. Using the polarization signatures discovered, it has been demonstrated that the polarimetric technique can be utilized for the discrimination of PM species. In the future, this technique may be exploited for developing sensors for bio-aerosol detection.

Acknowledgments

The funding for the instrumentation was made available by the Army's Defense University Research Instrumentation Program (DURIP). We are also very thankful to Art Lompado (Polaris Sensor Technologies) for his technical inputs and to Daniel Mork (HollisterStier Labs) for providing complimentary samples of pollen grains used in this study. Thanks are also due John Christy (Earth System Science Center, University of Alabama in Huntsville) and Mike Newchurch (Atmospheric Science Department, University of Alabama in Huntsville) for their support.

References

1. M. R. Hurst and E. Wilkins, "Chemical and biological warfare: should rapid detection techniques be researched to dissuade usage? A review," *Am. J. Appl. Sci.* **2**(4), 796–805 (2005).
2. A. H. Carrieri et al., "Infrared differential-absorption Mueller matrix spectroscopy and neural network-based data fusion for biological aerosol standoff detection," *Appl. Opt.* **49**(3), 382–393 (2010).
3. P. Raman, "Broadband (UV–VIS–NIR) Mueller matrix polarimeter," *Proc. SPIE* **8160**(1), 816013 (2011).
4. J. Eversole, "Point detection of threat aerosols: basic considerations and status," *Proc. SPIE* **5585**, 1–14 (2004).
5. A. H. Carrieri et al., "Photopolarimetric lidar duel-beam switching device and Mueller matrix standoff detection method," *J. Appl. Rem. Sens.* **1**(1), 013502 (2007).
6. J. M. Richardson and J. C. Aldridge, "The standoff aerosol active signature testbed (SAAST) at MIT Lincoln Laboratory," *Proc. SPIE* **5995**, 59950E (2005).
7. J. M. Richardson, J. C. Aldridge, and A. B. Milstein, "Polarimetric lidar signatures for remote detection of biological warfare agents," *Proc. SPIE* **6972**, 69720E (2008).
8. J. W. Snow et al., "Standoff polarimetric aerosol detection (SPADE) for biodefense," DTIC Document, Technical Report, Lincoln Laboratory, Massachusetts Institute of Technology (2005).
9. S. D. Mayor, S. M. Spuler, and B. M. Morley, "Scanning eye-safe depolarization lidar at 1.54 microns and potential usefulness in bioaerosol plume detection," *Proc. SPIE* **5887**, 58870N (2005).
10. R. J. Peralta et al., "Aerosol polarimetry sensor for the Glory Mission," *Proc. SPIE* **6786**, 67865L (2007).
11. D. J. Diner et al., "The Airborne Multiangle SpectroPolarimetric Imager (AirMSPI): a new tool for aerosol and cloud remote sensing," *Atmos. Meas. Tech. Discuss.* **6**, 1717–1769 (2013).
12. F. Snik et al., "SPEX: the spectropolarimeter for planetary exploration," *Proc. SPIE* **7731**, 77311B (2010).
13. G. Roy, X. Cao, and R. Bernier, "On linear and circular depolarization LIDAR signatures in remote sensing of bioaerosols: experimental validation of the Mueller matrix for randomly oriented particles," *Opt. Eng.* **50**(12), 126001 (2011).
14. F. M. D'Amico, R. P. Moon, and C. E. Davidson, "Aerosol identification using a hybrid active/passive system," *Proc. SPIE* **5887**, 58870P (2005).
15. P. Raman, K. Fuller, and D. Gregory, "Polarimetric discrimination of atmospheric particulate matter," *Proc. SPIE* **8364**, 83640D (2012).
16. D. H. Goldstein and E. Collett, *Polarized Light*, CRC, Boca Raton, FL (2003).
17. R. A. Chipman, "Polarimetry," in *Handbook of Optics*, 3rd ed., M. Bass, Ed., Vol. 1, pp. 15.1–15.41, McGraw Hill Inc., New York (1995).
18. R. M. A. Azzam, "Photopolarimetric measurement of the Mueller matrix by Fourier analysis of a single detected signal," *Opt. Lett.* **2**(6), 148–150 (1978).
19. D. H. Goldstein, "Mueller matrix dual-rotating retarder polarimeter," *Appl. Opt.* **31**(31), 6676–6683 (1992).
20. D. B. Chenault, J. L. Pezzaniti, and R. A. Chipman, "Mueller matrix algorithms," *Proc. SPIE* **1746**, 231–246 (1992).
21. D. H. Goldstein and R. A. Chipman, "Error analysis of a Mueller matrix polarimeter," *J. Opt. Soc. Am. A* **7**(4), 693–700 (1990).
22. S. Y. Lu and R. A. Chipman, "Interpretation of Mueller matrices based on polar decomposition," *J. Opt. Soc. Am. A* **13**(5), 1106–1113 (1996).
23. P. Raman, *Spectropolarimetric Characterization of Light Scattering Materials*, University of Alabama in Huntsville, Ph.D. Dissertation (2012).
24. "Optical Glass Data Sheet," www.schott.com/advanced_optics/us/abbe_datasheets/schott_datasheet_all_us.pdf (2013).
25. D. Greenberg et al., "Identifying experimental surrogates for Bacillus anthracis spores: a review," *Invest. Genet.* **1**(1), 4 (2010).
26. U. S. Government, *Extinction, Absorption, Scattering, and Backscatter for Aerosolized Bacillus Subtilis Var Niger Endospores from 3 to 13 Micrometers*, General Books LLC (2012).
27. V. Sivaprakasam et al., "Optical characterization of individual bioaerosols," in *Electromagnetic and Light Scattering XII*, K. Muinonen et al., Ed., Vol. 1, p. 282, Helsinki University, Helsinki (2010).
28. P. S. Tuminello et al., "Optical properties of *Bacillus subtilis* spores from 0.2 to 2.5 μm," *Appl. Opt.* **36**(13), 2818–2824 (1997).
29. K. Faegri, P. E. Kaland, and K. Krzywinski, *Textbook of Pollen Analysis*, Blackburn Press, Caldwell, NJ (2000).
30. R. O. Kapp, *Pollen and Spores*, W.C. Brown, Iowa (1969).
31. P. D. Moore, J. A. Webb, and M. E. Collinson, *Pollen Analysis*, Blackwell Science (1991).
32. R. P. Wodehouse, *Pollen Grains: Their Structure, Identification, and Significance in Science and Medicine*, Hafner Pub. Co. (1959).
33. J. H. Seinfeld and S. N. Pandis, *Atmospheric Chemistry and Physics: From Air Pollution to Climate Change*, Wiley-Interscience, New York, NY (2012).
34. J.-C. Raut and P. Chazette, "Retrieval of aerosol complex refractive index from a synergy between lidar, sunphotometer and in situ measurements during LISAIR experiment," *Atmos. Chem. Phys.* **7**(11), 2797–2815 (2007).
35. E. Dinar et al., "The complex refractive index of atmospheric and model humic-like substances (HULIS) retrieved by a cavity ring down aerosol spectrometer (CRD-AS)," *Faraday Discuss.* **137**, 279–295 (2008).

Prashant Raman graduated with a PhD in optical science and engineering from the University of Alabama in Huntsville in 2012. His dissertation was titled "Spectropolarimetric Characterization of Light Scattering Materials" and advised by Dr. Kirk Fuller.

Kirk A. Fuller has a PhD in physics from Texas A&M University. He has worked extensively in the fields of electromagnetic theory of optically coupled nano- and microstructures, spectroscopy, radiative transfer, optical properties of materials, and aerosol science. Before joining UAH, he was a National Research Council postdoc at the White Sands Missile Range, and then a Research Scientist with the Atmospheric Science Department at Colorado State University. He has also served as a consultant for NASA, NIST, the Army Research Laboratory, the EPA and various biomedical and solar power companies. He has authored 30+ peer-reviewed journal articles and book chapters.

Don A. Gregory is professor of physics at the University of Alabama in Huntsville and also holds appointments in the optical science and engineering and the materials science programs. Previously, he was a supervisory research physicist and chief of the photonics and laser sciences branch of the US Army Missile Command, Redstone Arsenal, Alabama. Professor Gregory has more than 120 refereed publications in the fields ranging from fundamental optical properties of materials to optical pattern recognition. He has been named Outstanding Teacher of the Year at the University of Alabama and is a winner of the Fink prize for outstanding IEEE publication. He has graduated 23 MS students (thesis) and 21 PhDs since joining UAH in 1992.